Facilitating Uniform Large-scale MoS_2, WS_2 Monolayers and Their Heterostructures Through Van der Waals Epitaxy

Chung-Che Huang[*1], He Wang[2], Yameng Cao[3], Ed Weatherby[1], Filipe Richheimer[3], Sebastian Wood[3], Shan Jiang[4], Daqing Wei[4], Yongkang Dong[5], Xiaosong Lu[6], Pengfei Wang[7], Tomas Polcar[2] and Daniel W. Hewak[1]*

[1]Chung-Che Huang, Ed Weatherby, Daniel W. Hewak, Optoelectronics Research Centre, University of Southampton, Southampton, SO17 1BJ, United Kingdom

[2]He Wang, Tomas Polcar, nCAT, University of Southampton, SO17 1BJ, United Kingdom

[3]Yameng Cao, Filipe Richheimer, Sebastian Wood, National Physical Laboratory, Teddington, TW11 0LW, United Kingdom

[4]Shan Jiang, Daqing Wei, School of Materials Science and Engineering, Harbin Institute of Technology, 150001 Harbin, China.

[5]Yongkang Dong, National Key Laboratory of Science and Technology on Tunable Laser, Harbin Institute of Technology, 150001 Harbin, China.

[6]Xiaosong Lu, School of Physics and Electronic Engineering, Jiangsu Normal University, 221116 Xuzhou, China

[7]Pengfei Wang, Key Laboratory of In-fiber Integrated Optics of Ministry of Education, College of Science, Harbin Engineering University, 150001 Harbin, China

*Corresponding author: cch@orc.soton.ac.uk

KEYWORDS: MoS_2, WS_2, heterostructures, Van der Waals epitaxy, transition metal dichalcogenides, nanoelectronics, nanophotonics

ABSTRACT: The fabrication process for the uniform large-scale MoS_2, WS_2 transition metal dichalcogenides (TMDCs) monolayers and their heterostructures has been developed by Van der Waals epitaxy (VdWE) through the reaction of $MoCl_5$ or WCl_6 precursors and the reactive gas H_2S to form MoS_2 or WS_2 monolayers, respectively. The heterostructures of MoS_2/WS_2 or WS_2/MoS_2 can be easily achieved by changing the precursor from WCl_6 to $MoCl_5$ once the WS_2 monolayer has been fabricated or switching the precursor from $MoCl_5$ to WCl_6 after the MoS_2 monolayer has been deposited on the substrate.

These VdWE-grown MoS_2, WS_2 monolayers and their heterostructures have been successfully deposited on Si wafer with 300 nm SiO_2 coating (300 nm SiO_2/Si), quartz glass, fused silica and sapphire substrates using the protocol we have developed. We have characterized these TMDCs materials with a range of tools/techniques including scanning electron microscope (SEM), X-ray photoelectron spectroscopy (XPS), micro-Raman, photoluminescence (PL), atomic force microscopy (AFM), transmission electron microscope (TEM), energy-dispersive X-ray spectroscopy (EDX) and selected area electron diffraction (SAED). The band alignment and large-scale uniformity of MoS_2/WS_2 heterostructures have also been evaluated with PL spectroscopy. This process and resulting large-scale MoS_2, WS_2 monolayers and their heterostructures have demonstrated promising solutions for the applications in next generation nanoelectronics, nanophotonics and quantum technology.

1. Introduction

Transition metal di-chalcogenides (TMDCs) such as MoS_2, $MoSe_2$, WS_2 and WSe_2 are two-dimensional (2D) Van der Waals (VdW) layered materials. Unlike graphene, TMDCs are semiconductors that could offer, in particular, bandgap engineering properties through both their chemical compositions and number of layers.[1,2] The applications of the use of TMDCs are very promising in the area of transistors,[1] light emitting diodes,[3,4] photodetectors,[5] sensing[6,7] and memory devices,[8] as well as the potential substitution for Si in conventional electronics[9] and of organic semiconductors in wearable and flexible systems.[10]

The current fabrication processes for these emerging TMDCs include exfoliation,[1,11] hydrothermal process,[12] physical vapour deposition,[13] transition metal oxides sulfurization,[14] electrochemical deposition,[15] thermolysis of transition metal chalcogenide compounds[16,17] and chemical vapour deposition (CVD).[18–20] The majority of TMDCs fabricated by these techniques are in the form of flakes with the sizes in the range of a few hundred square micrometers in area. However, the challenge for large-scale fabrication of TMDCs is to provide a reliable complementary metal-oxide-semiconductor (CMOS)-compatible process for the integration of 2D TMDCs on a desired wafer-scale substrate.[2,21]

We have been working on the synthesis of chalcogenide materials using vapour phase deposition processes[22–27] such as CVD, atomic layer deposition (ALD) and VdWE. Apart from offering conformal coating and stoichiometric control of thin film compositions, these processes are scalable and compatible with a range of substrates. In particular, VdWE has been demonstrated to carry out the epitaxy of layered TMDCs on the substrates even with lattice constants mismatch.[28–30] In this paper, we have developed the fabrication process for the uniform large-scale MoS_2, WS_2

TMDCs monolayers and their heterostructures by VdWE through the reaction of $MoCl_5$ or WCl_6 precursors and the reactive gas H_2S to form MoS_2 or WS_2 monolayers, respectively. The heterostructures can easily be achieved by changing the precursor from WCl_6 to $MoCl_5$ once the initial WS_2 monolayer is fabricated or switching the precursor from $MoCl_5$ to WCl_6 after MoS_2 monolayer has been deposited on the substrate.

2. Experimental Setup

The VdWE apparatus we developed is shown schematically in Figure 1. The precursors, $MoCl_5$ (99.6 % pure from Alfa Aesar) and WCl_6 (99.9 % pure from Sigma-Aldrich) were kept in the bubblers inside the dry N_2 purged glovebox. The $MoCl_5$/WCl_6 vapours were delivered by high purity argon gases through the mass flow controllers (MFCs) to the VdWE apparatus with the flow rate of 300 standard cubic centimeters per minute (sccm). The system equipped with a bespoke furnace with three heating zones, individually controlled by proportional integral derivative (PID) controllers, with maximum temperature of 1200 ^oC and temperature uniformity of ± 3 ^oC can be achieved over 450mm length to facilitate the uniform large-scale deposition of TMDC monolayers. The reactive gases were H_2S mixed with another argon gas through individual MFCs with the flow rates of 50 sccm and 300 sccm respectively. All the gases were purified by passing through the individual point of use purifiers (SAES MicroTorr) and the moisture level of all gases were monitored by the dewpoint sensors (Michell Instrument Pura pure gas trace moisture transmitters) before entering the VdWE reactor. The typical moisture readings of the Ar and H_2S/Ar mixture were -99.6 ^oCdp (~7 ppb) and -90.2 ^oCdp (~42 ppb) respectively. The process was set at 30 mBar using a pump (Vacuubrand MV 10C NT Vario) with a pressure controller for the entire deposition. With this VdWE apparatus, uniform large-scale TMDCs monolayers have been successfully

deposited on various substrates, including 300 nm SiO_2/Si, quartz glass, fused silica or c-plane sapphire. The sizes of the substrates were typically 25 mm × 25 mm, however up to a 40 mm × 100 mm substrate can be loaded into the VdWE apparatus, which consists of a 50 mm O.D. × 1000 mm long quartz reaction tube. The substrates were cleaned with acetone using an ultrasonic bath at 50 ºC for 10 minutes, then rinsed with isopropanol, deionized water and subsequently blow dried with N_2 gas. The temperatures for the growth of MoS_2 and WS_2 monolayers were set at 850 ºC and 900 ºC respectively. The reactive H_2S gas and $MoCl_5$/WCl_6 precursors were introduced to VdWE system once the furnace reached the set temperature. MoS_2/WS_2 were formed after the $MoCl_5$/WCl_6 precursors met with H_2S gas after the injection tube inside the quartz reaction tube. With sufficient amount of $MoCl_5$/WCl_6 precursors flux, MoS_2/WS_2 monolayers can be uniformly deposited on the substrates and the resulting MoS_2/WS_2 monolayers tend to be polycrystalline due to the high flux of precursors. Although the substrates might affect the deposition of TMDCs, we didn't see significant differences in quality of the MoS_2, WS_2 monolayers and their heterostructures on the substrates we used. This is probably due to the VdWE process can overcome the mismatch of substrate lattice constants. To achieve uniform MoS_2 and WS_2 monolayers, a deposition time of 4 minutes and 5 minutes was required for the MoS_2 and WS_2 monolayers respectively.

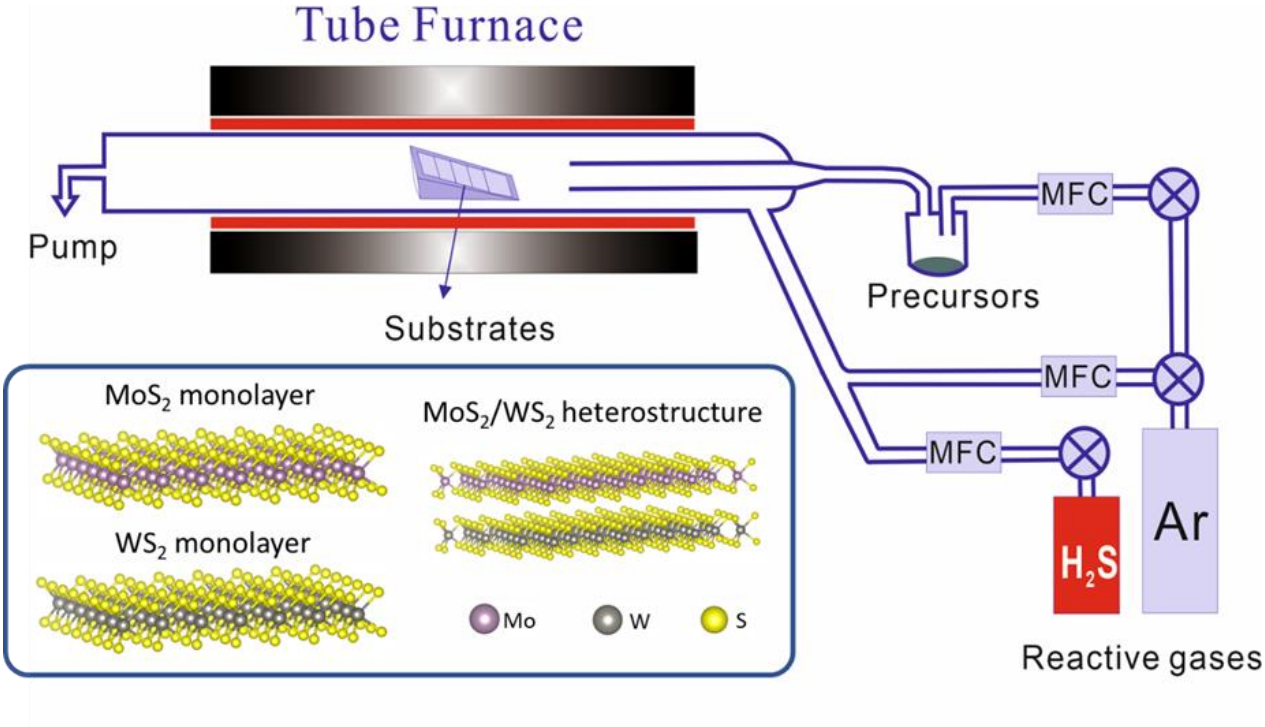

Figure 1. Schematic VdWE apparatus for the fabrication of MoS_2, WS_2 and their heterostructures.

3. Results and Discussion

We have achieved large area MoS_2 and WS_2 monolayers as shown in Figure 2(a) on quartz glass and in Figure 2(b) on 300 nm SiO_2/Si substrates respectively. These results have demonstrated that wafer scale deposition of MoS_2 and WS_2 monolayers is feasible through a modification of the VdWE system with a larger reaction chamber.

Raman spectroscopy was carried out for the initial study of the quality of the VdWE-grown MoS_2 and WS_2 monolayers on quartz glass and 300 nm SiO_2/Si substrates using a Renishaw Ramascope. 532 nm and 473 nm excitation lasers were used to excite the MoS_2 monolayer and

WS_2 monolayer samples and the Raman shift spectra were shown in Figure 2(c) and 2(d) for MoS_2 and WS_2 respectively. As shown in Figure 2(c), two MoS_2 Raman peaks, E^1_{2g} in-plane phonon mode and A_{1g} out-of-plane phonon mode were revealed at 384.0 cm^{-1} and 403.7 cm^{-1} respectively. The number of MoS_2 layers can be evaluated by the energy difference between these two Raman peaks (Δ).[31] From Figure 2(c), the Δ value is 19.7 cm^{-1} for the VdWE-grown MoS_2 monolayer, which is similar to the reported literature.[31] On the other hand, in order to reduce the second order 2LA phonon mode in the WS_2 Raman measurement,[32] a 473 nm laser was used to reveal two WS_2 Raman peaks, E^1_{2g} and A_{1g} at 359.2 cm^{-1} and 419.4 cm^{-1} respectively. Again, the Δ value can be also used to evaluate the number of WS_2 layers.[32] From Figure 2(d), the Δ value is 60.2 cm^{-1} for the VdWE-grown WS_2 monolayer, which is also matching with the literature.[32]

The photoluminescence (PL) spectroscopy from the VdWE-grown MoS_2 monolayer on quartz glass and WS_2 monolayer on 300 nm SiO_2/Si substrates were studied using the same Raman microscope. Two excitonic peak A and peak B at 666.3 nm (1.86 eV) and 614.3 nm (2.02 eV) respectively were found in the PL spectrum of VdWE-grown MoS_2 monolayer on quartz glass substrate as shown in Figure 2(e). These results are similar to the reported literature.[33] On the other hand, the PL spectrum of VdWE-grown WS_2 monolayer on 300 nm SiO_2/Si substrate confirmed the direct band emission at 616.1 nm (2.01 eV) as shown in Figure 2(f). Again, this result agrees with the literature reports.[34]

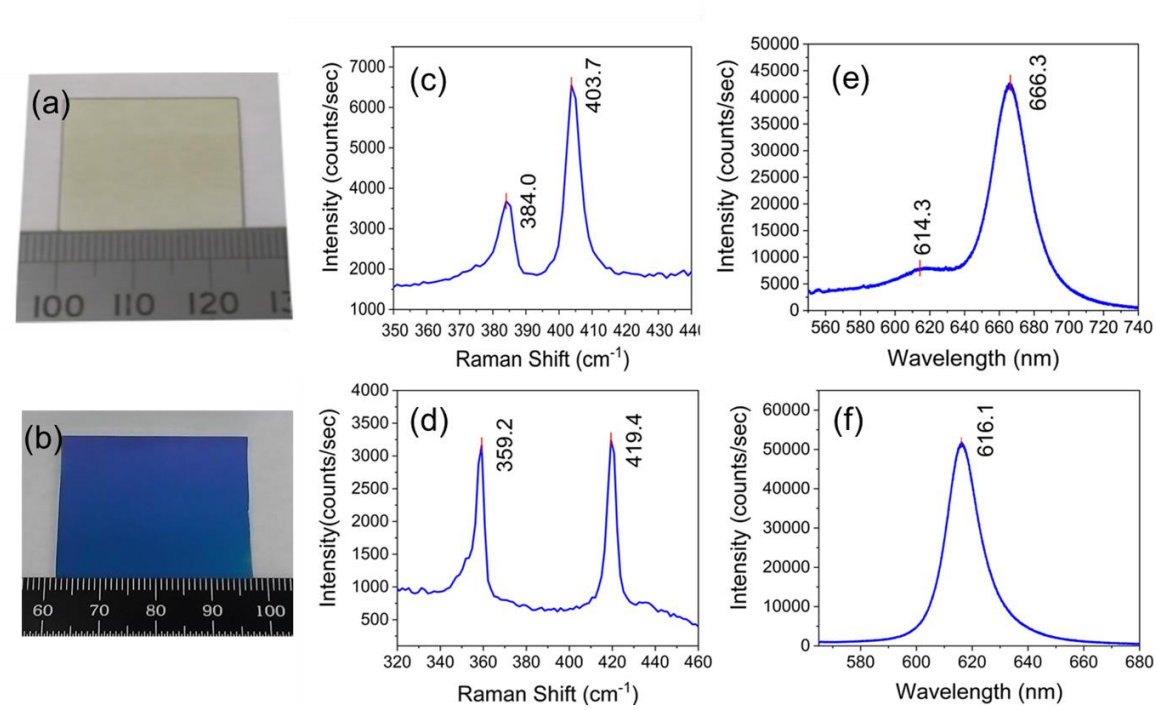

Figure 2. (a) photo of VdWE-grown MoS_2 monolayer on quartz glass substrate, (b) photo of WS_2 monolayer on 300 nm SiO_2/Si substrate, (c) Raman spectrum of VdWE-grown MoS_2 monolayer on quartz glass (with 532 nm excitation laser), (d) Raman spectrum of VdWE-grown WS_2 monolayer on 300 nm SiO_2/Si substrate (with 473 nm excitation laser), (e) Photoluminescence spectrum of VdWE-grown MoS_2 monolayer on quartz glass (with 532 nm excitation laser), and (f) Photoluminescence spectrum VdWE-grown WS_2 monolayer on 300 nm SiO_2/Si substrate (with 532 nm excitation laser).

Furthermore, the PL spectra mapping was carried out to study the uniformity of large-scale VdWE-grown WS_2 monolayer on a 300 nm SiO_2/Si substrate. The map of the PL emission at 2.01 eV shown in Figure 3 reveals a very good uniformity of the WS_2 monolayer over an area of 35 mm × 50 mm. This has been achieved by our in-house built apparatus and this process could be scalable for even large wafer-scale process if a larger reactor is available.

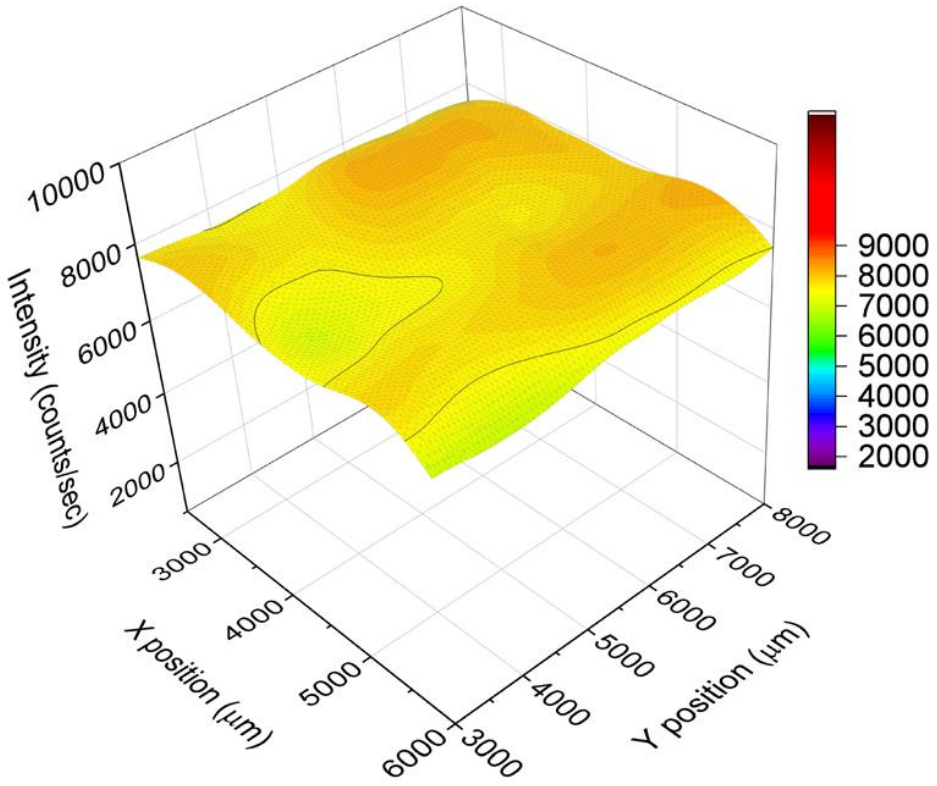

Figure 3. Photoluminescence spectra mapping at 2.01 eV of VdWE-grown WS_2 monolayer on 300 nm SiO_2/Si substrate.

X-ray photoelectron spectroscopy (XPS) was carried out to study the compositions of these VdWE-grown MoS_2 and WS_2 monolayers using a Thermo Scientific Theta Probe XPS System. For MoS_2 monolayer, two core levels, Mo 3d and the S 2p, have been investigated. As shown in Figure 4 (a), two MoS_2 peaks, Mo (IV) $3d_{3/2}$ and Mo (IV) $3d_{5/2}$, were found at 233.0 eV and 229.9 eV respectively. In the same spectrum, S 2s peak was observed at 227.2 eV and a peak at 236.0 eV was assigned to the Mo (VI) $3d_{3/2}$ indicating a small amount of oxidation which resulted from the sample being exposed to the ambient environment. It should be noted that a Mo (VI) $3d_{5/2}$ peak

overlaps with Mo (IV) $3d_{3/2}$ at 233.0 eV. For the MoS_2 S 2p core level, two peaks labelled in Figure 4(b) as S $2p_{1/2}$ and S $2p_{3/2}$ corresponding to MoS_2 were found at 163.9 eV and 162.7 eV respectively. In addition, with semi-quantitative method to investigate the ratio of elements, the atomic ratio of S/Mo was found to be approximately 1.93 with slight S deficiency. These results are in line with literature.[35] On the other hand, for the WS_2 monolayer, two core levels, W 4f and S 2p, have been studied. As shown in Figure 4(c), two WS_2 peaks, W(IV) $4f_{5/2}$ and W(IV) $4f_{7/2}$ were found at 35.2 eV and 33.0 eV respectively and in the same spectrum, two peaks at 38.5 eV and 36.3 eV were assigned to W(VI) $4f_{5/2}$ and W(VI) $4f_{7/2}$ which again indicate a small amount of oxidation. It should also be noted that W(VI) $4f_{5/2}$ peak overlaps with W(VI) $5p_{3/2}$ at 38.5 eV. For the WS_2 S 2p core level, two peaks labelled in Figure 4(d) as S $2p_{1/2}$ and S $2p_{3/2}$ corresponding to WS_2 were found at 164.0 eV and 162.8 eV respectively. In addition, the atomic ratio of S/W was found to be approximately 1.96 with slight S deficiency. These results also agree with literature very well.[36]

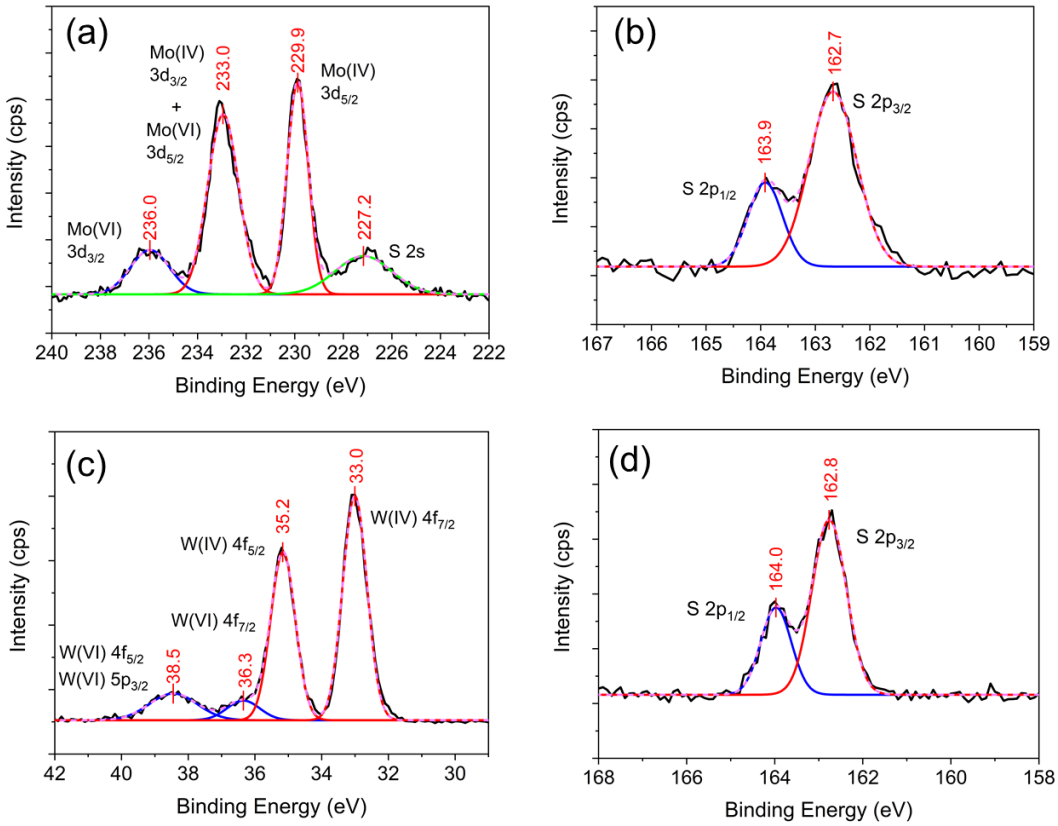

Figure 4. XPS measurements of VdWE-grown MoS_2 and WS_2 monolayers (a) Mo 3d scan of MoS_2 monolayer (b) S 2p scan of MoS_2 monolayer (c) W 4f scan of WS_2 monolayer (d) S 2p scan of WS_2 monolayer on 300 nm SiO_2/Si substrate.

In order to evaluate the crystalline structures of these VdWE-grown MoS_2 or WS_2 monolayers, commercially available 40 nm SiO_2 membranes TEM grids with 200 nm thick Si_3N_4 supporting frames (PELCO® Silicon Dioxide Support Films for TEM) were used to directly deposit these MoS_2 and WS_2 monolayers on this type of TEM grids. The optical image of as-deposited MoS_2 monolayer on TEM grid is shown in Figure 5(a) with a 532 nm laser spot on the center of the MoS_2/40 nm SiO_2 membrane. The Raman spectrum of the MoS_2 monolayer/40 nm SiO_2 sample is

shown in Figure 5(b). Again, two characteristic MoS_2 Raman peaks, E^1_{2g} and A_{1g} modes were found at 385.8 cm^{-1} and 402.9 cm^{-1} respectively with the Δ value of 17.1 cm^{-1} for the VdWE-grown MoS_2 monolayer on 40 nm SiO_2 membrane TEM grid. It should be noted that the Δ value appears less than that typically reported for the MoS_2 monolayer due to the weak Raman signal from the sample which increased the experimental uncertainty. In addition, the smaller Δ value could be also due to softening of the A_{1g} mode. The E^1_{2g} mode is insensitive to substrates but the A_{1g} mode is sensitive to charge density.[37] Despite these issues however, the monolayer nature has been revealed. In the PL spectrum, shown in Figure 5(c), only the excitonic peak A at 661.1 nm (~1.88 eV) was found for this sample on 40 nm SiO_2 TEM membrane whereas the B exciton could be only weakly detected. The sample was inspected by scanning TEM with a high-angle-annular-dark-field (HAADF-STEM), using FEI Talos F200x, USA, operating at 200 kV and equipped with an energy-dispersive X-ray spectrometer (EDX) system. The TEM image shown in Figure 5(d) has revealed the polycrystalline nature of VdWE-grown MoS_2 monolayer on 40 nm SiO_2 TEM membrane and the grain sizes are around 10 nm. The selected area electron diffraction (SAED) patterns shown in Figure 5(e) also confirmed the polycrystalline structures of this MoS_2 monolayer. The elemental mapping was carried out in the STEM-EDX mode. As shown in Figure 5(f) and 5(g), the Mo and S respectively were quite uniform over the measured area.

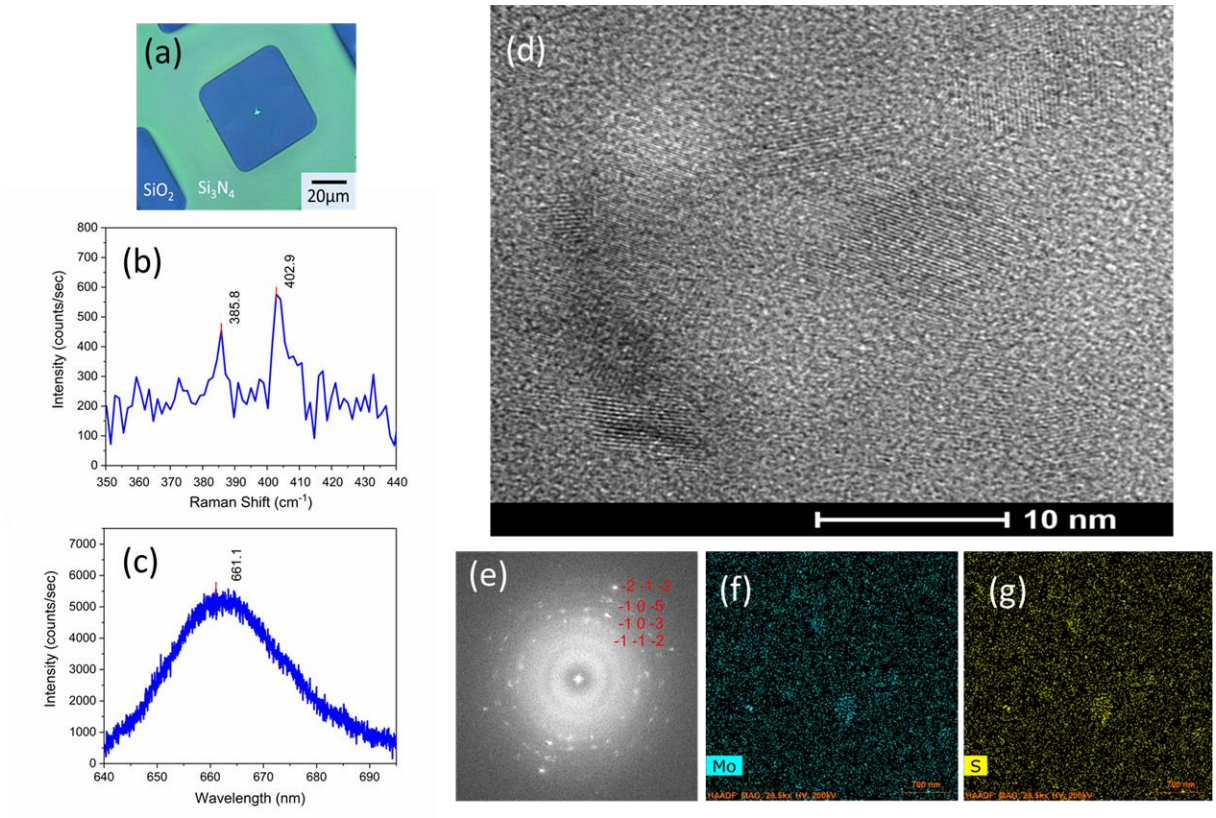

Figure 5. TEM measurements of VdWE-grown MoS_2 monolayer on 40 nm SiO_2 membrane/Si_3N_4/Si TEM grid (a) photo of sample with a 532 nm laser spot (b) Raman spectrum of VdWE-grown MoS_2 monolayer sample (c) PL spectrum of VdWE-grown MoS_2 monolayer sample (d) TEM image of VdWE-grown MoS_2 monolayer sample (e) Selected area electron diffraction (SAED) patterns of VdWE-grown MoS_2 monolayer sample (f) Energy-dispersive X-ray spectroscopy (EDX) mapping of Mo atom on the selected area of MoS_2 monolayer sample (g) EDX mapping of S atom on the selected area of MoS_2 monolayer sample.

The optical image of as-deposited WS_2 monolayer on TEM grid is shown in Figure 6(a) with a 532 nm laser spot on the center of the WS_2/40 nm SiO_2 membrane. The Raman spectrum of WS_2 monolayer/40 nm SiO_2 sample is shown in Figure 6(b). Two WS_2 Raman peaks, 2LA phonon

mode and A_{1g} mode were found at 352.9 cm^{-1} and 416.0 cm^{-1} respectively. In addition, as shown in Figure 6(c), the direct band emission at 620.0 nm (2.00 eV) was revealed from the PL spectrum. Again, these results agree with the literature reports.[26,34] The TEM image shown in Figure 6(d) has revealed the polycrystalline nature of VdWE-grown WS_2 monolayer on 40 nm SiO_2 TEM membrane and the grain sizes are around 10 nm. The selected area electron diffraction (SAED) patterns shown in Figure 6(e) also confirmed the polycrystalline structures of this WS_2 monolayer. The elemental mapping was carried out in the STEM-EDX mode. As shown in Figure 6(f) and 6(g), the W and S respectively were quite uniform over the measured area.

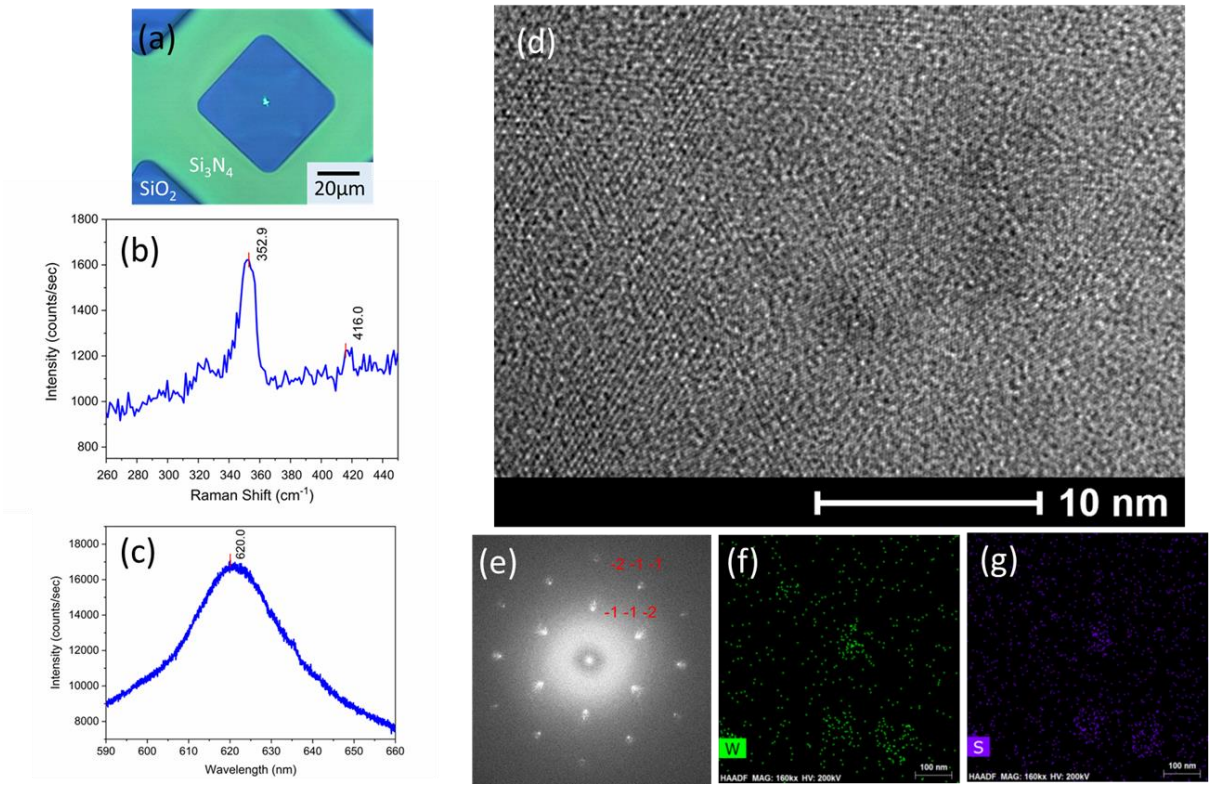

Figure 6. TEM measurements of VdWE-grown WS_2 monolayer on 40 nm SiO_2 membrane/Si_3N_4/Si TEM grid (a) photo of sample with a 532 nm laser spot (b) Raman spectrum of VdWE-grown WS_2 monolayer sample (c) PL spectrum of VdWE-grown WS_2 monolayer sample (d) TEM image of VdWE-grown MoS_2 monolayer sample (e) Selected area electron

diffraction (SAED) patterns of VdWE-grown WS_2 monolayer sample (f) Energy-dispersive X-ray spectroscopy (EDX) mapping of Mo atom on the selected area of WS_2 monolayer sample (g) EDX mapping of S atom on the selected area of WS_2 monolayer sample.

A MoS_2/WS_2 monolayer heterostructure on the fused silica substrate was prepared for further investigation with the abovementioned VdWE process. WS_2 monolayer was firstly grown on 25 mm x 25 mm fused silica substrate, followed by the second MoS_2 monolayer grown on the top of WS_2 monolayer/fused silica sample. As the Raman spectrum shown in Figure 7(a), two typical MoS_2 E^1_{2g} and A_{1g} peaks are revealed along with the WS_2 peaks labeled as $WS_2(2LA\text{-}2E^2_{2g})$, $WS_2(2LA\text{-}E^2_{2g})$, $WS_2(2LA+E^2_{2g})$ and $WS_2(A_{1g})$. The band alignment of MoS_2/WS_2 monolayer heterostructures has also been evaluated with the PL spectrum shown in Figure 7(b) which revealed that the VdWE-grown MoS_2/WS_2 on fused silica sample forms a type-II heterojunction with more detailed discussion in the supporting information.

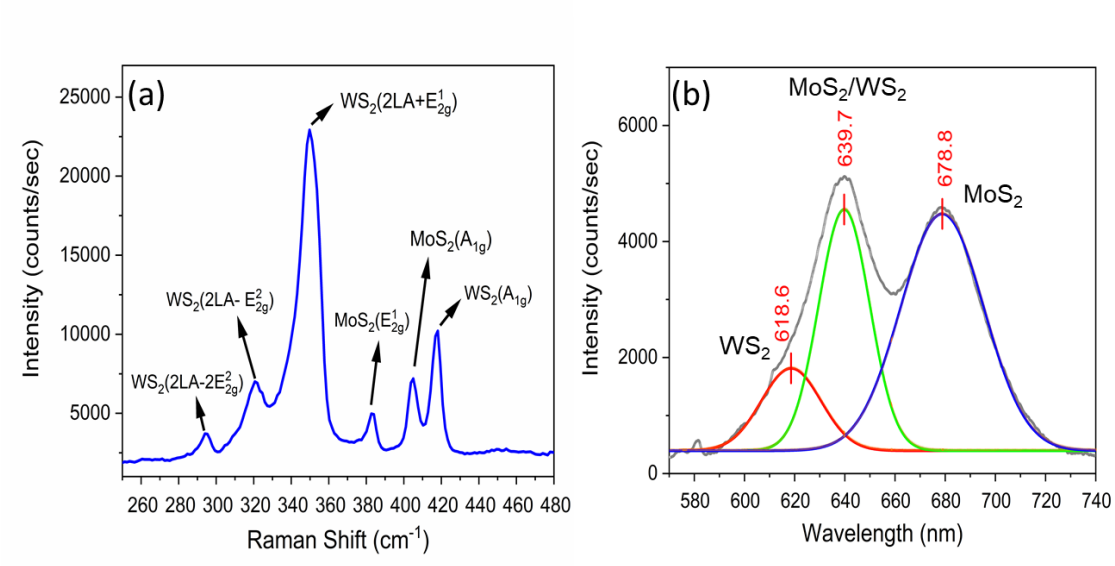

Figure 7. (a) Raman spectrum of MoS_2/WS_2 heterostructure on fused silica (b) PL spectrum of MoS_2/WS_2 heterostructure on fused silica.

It is very difficult to see the contrast between MoS_2 and WS_2 monolayers in the VdWE-grown MoS_2/WS_2 heterostructures since the VdWE provide the uniform and continuous atomically thin TMDCs. To visualize the MoS_2/WS_2 heterostructures, MoS_2 monolayer flakes were prepared on a 300 nm SiO_2/Si substrate with the conventional CVD process,[38] followed by the coating with a uniform WS_2 monolayer with the VdWE process. The structure of these VdWE-grown WS_2 continuous film / CVD-grown MoS_2 flakes heterostructures illustrated in Figure S1(a) with the optical image in Figure S1(b). The detailed characterizations of AFM, Raman, XPS and PL are discussed in the supporting information (Fig. S1).

The spatial uniformity in the VdWE WS_2/MoS_2 heterostructures are investigated by PL mapping. A recent report[39] has shown that the PL uniformity in exfoliated 2D materials is strongly correlated to the uniformity in the spectral properties, such as the emission energy and spectral weighting. A similar analysis is applied here to investigate the uniformity of the heterostructures in terms of the emission energies of each of the corresponding layers in the heterostructure and offer a baseline for comparisons with future studies. Since there is an abundance of heterostructures flakes, the uniformity analysis extends naturally from intra-flake (within one heterostructure flake) to inter-flake (between multiple flakes), that could provide additional insight for future growth optimizations. The monolayer MoS_2 flakes on this sample are mostly equilateral triangles, hexagrams and partial hexagrams of various sizes and orientations. To sample this geometric distribution, an area is selected using optical microscopy, shown in Figure 8 (l) that

contains five numerically labelled flakes, with flakes F1, F2 and F5 being triangles, F4 being a hexagram and F3 being a partial hexagram, the regions outside of these flakes corresponds to the VdWE WS_2 monolayer film. A PL map of the whole region was acquired, using a Horiba LabRAM spectrometer, with 532 nm Laser (637 kW/cm^2, 5 seconds integration time), focused through a 100x 0.95 NA objective lens, and the emission dispersed with a 600 lines/mm grating. The mapped region is 40 μm by 40 μm in size and the raster scan step size is 0.5 μm. Maps of individual heterostructure flakes were then isolated from the recorded PL map by a MATLAB program. From Figure 8 (m) the WS_2 region has a single peak at ≈ 2.00 eV (WS_2 exciton), while two peaks appear in the heterostructure spectrum at ≈ 1.84 eV (MoS_2 exciton) and ≈ 1.98 eV (WS_2 exciton).

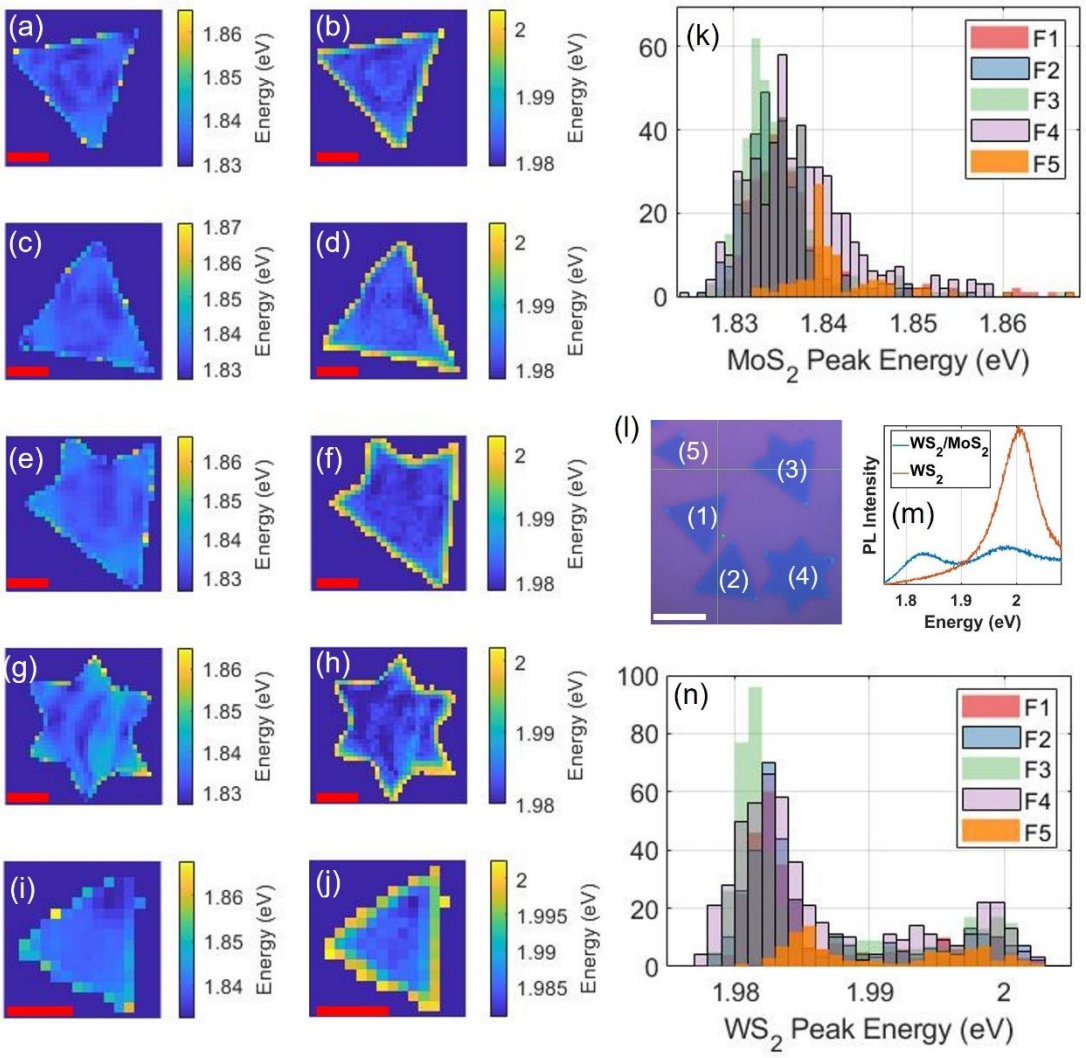

Figure 8. Intra-flake and inter-flake PL spatial and spectral uniformity analysis for five different flakes, as indicated by the optical image (l) with a white scale bar representing 10 µm, on the sample with VdWE-grown WS_2 monolayer on CVD-grown MoS_2 monolayer flakes heterostructure on 300 nm SiO_2/Si. (a, c, e, g, i) Maps of fitted MoS_2 peak energies for flakes F1-F5, with red scale bars representing 5 µm. (b, d, f, h, j) Maps of fitted WS_2 peak energies for flakes F1-F5, with red scale bars representing 5 µm. (k) MoS_2 and (n) WS_2 peak energy histograms for

F1-F5 plotted on top of each other, all histograms have energy bins 1 meV wide. Typical PL spectrum measured from the heterostructure and the surrounding WS_2 are also plotted in (m).

Spatial variations in emission energy are apparent for both MoS_2 and WS_2, as revealed from the peak energy maps in Figure 8 (a-j). Across all flakes, the peak energy from both materials exhibits similar spatial patterns, where a local area that indicate blueshifts (or redshift) in one material corresponds to blueshifts (or redshift) in the other at the same spatial location. Though for the MoS_2 peak, its intra-flake energy range, taken as the 95% confidence region in the histograms shown in Figure 8 (k) is up to ≈ 10 meV, compared to ≈ 4 meV for that of WS_2, from Figure 8 (n). There is a pronounced edge-effect for WS_2, less so for MoS_2, where the peak appears to exhibit significant blueshift at the edge of all heterostructures measured. This also explains the differences which are apparent from the histograms plotted in Figure 8(k) and Figure 8(n), showing largely monomodal distribution for MoS_2 and bimodal for WS_2. The two modes in Figure 8(n) corresponds to the interior and edge peak energy distributions for WS_2 and the means of these two modes are separated by ≈ 17 meV. The fact that all measured flakes exhibit similar behavior, independent of the flake size, geometry and orientation suggests that strain is the likely mechanism to explain this, as its magnitude could be changed at the edge WS_2 layer as its substrate changes from MoS_2 to silicon dioxide. For MoS_2 the peak shift at the flake-edge is much less pronounced, up to 5 meV on average, which is smaller than the inhomogeneity in the MoS_2 peak energy of ≈ 10 meV, so that only in the smallest flake measured (F5) this modal separation is apparent. Overall, the inter-flake uniformity is well-behaved, i.e., does not fluctuate significantly from flake to flake regardless of size geometry and orientation, which suggests that the growth-process has good reproducibility between heterostructures. The intra-flake uniformity is also well-behaved if the edge-effects can

be ignored, which could be valid for large area heterostructure flakes. However, charge transport phenomena at the edge that change this behaviour, which could be an interesting avenue to explore in a future study with a device, as PL-uniformity analysis alludes to the optical transport phenomena only.

4. Conclusion

In conclusion, we have demonstrated a scalable fabrication process for TMDC monolayers and their heterostructures by Van der Waals epitaxy. These VdWE-grown MoS_2, WS_2 monolayers and their heterostructures have been successfully deposited on CMOS-compatible substrates, such as 300 nm SiO_2/Si wafer, quartz glass, fused silica and sapphire. Detailed characterizations of these TMDCs materials have been carried out with SEM, AFM, XPS, micro-Raman, micro-PL, TEM, EDX and SAED techniques and the band alignment and large-scale uniformity of MoS_2/WS_2 heterostructures has also been evaluated with spatially-resolved PL spectroscopy. These results have demonstrated not only the excellent characteristics of MoS_2 and WS_2 monolayers with large-scale uniformity but also the feasibility of large-scale TMDCs heterostructures can be achieved by the VdWE in this work. We believe this process and resulting large-scale MoS_2, WS_2 monolayers and their heterostructures have demonstrated promising solutions for the applications in next generation nanoelectronics, nanophotonics and quantum technology.

Acknowledgements

The authors would like to acknowledge Dr. Yohann Franz for Raman measurement with 473nm laser at Diamond Light Source and the technical assistance of Mr Chris Craig. The 2D materials

work is funded by the Engineering Physical Sciences Research Council through the Chalcogenide Photonic Technologies (EPSRC EP/M008487/1) and the Future Photonics Manufacturing Hub (EPSRC EP/N00762X/1) at the University of Southampton, United Kingdom. This work received funding from the UK Government's Department for Business, Energy and Industrial Strategy (BEIS) through the UK's National Measurement System programmes at the National Physical Laboratory, United Kingdom.

Author Contributions

C.-C.H. conceived the VdWE apparatus designs and carried out initial fabrication, testing and characterizations. H.W. prepared CVD-grown single crystals and 2D heterostructures and characterized these materials. Y.C., F.R and S.W. preformed the characterizations of WS_2/MoS_2 heterostructures. E.W. assisted in the construction of VdWE apparatus. S.J., D.W., Y.D., X.L. and P.W. assisted in the TEM measurements. T.P., D.W., P.W., Y.C. and C.-C.H coordinated the research collaboration. Y.C. and C.-C.H. wrote manuscript and all authors contributed to technical discussions and paper writing.

Supporting Information Available

Additional band structure calculations of VdWE-grown MoS_2/WS_2 on fused silica sample and detailed characterization of VdWE-grown WS_2/CVD-grown MoS_2 heterostructures on 300nm SiO_2/Si substrate.

REFERENCES

(1) Radisavljevic, B.; Radenovic, A.; Brivio, J.; Giacometti, V.; Kis, A. Single-Layer MoS2 Transistors. *Nature Nanotechnology* **2011**, *6* (3), 147–150. https://doi.org/10.1038/nnano.2010.279.

(2) Wang, Q. H.; Kalantar-Zadeh, K.; Kis, A.; Coleman, J. N.; Strano, M. S. Electronics and Optoelectronics of Two-Dimensional Transition Metal Dichalcogenides. *Nature Nanotechnology*. Nature Publishing Group **2012**, pp 699–712. https://doi.org/10.1038/nnano.2012.193.

(3) Sundaram, R. S.; Engel, M.; Lombardo, A.; Krupke, R.; Ferrari, A. C.; Avouris, P.; Steiner, M. Electroluminescence in Single Layer MoS2. *Nano Letters* **2013**, *13* (4), 1416–1421. https://doi.org/10.1021/nl400516a.

(4) Cheng, R.; Li, D.; Zhou, H.; Wang, C.; Yin, A.; Jiang, S.; Liu, Y.; Chen, Y.; Huang, Y.; Duan, X. Electroluminescence and Photocurrent Generation from Atomically Sharp WSe2/MoS2 Heterojunction p-n Diodes. *Nano Letters* **2014**, *14* (10), 5590–5597. https://doi.org/10.1021/nl502075n.

(5) Lopez-Sanchez, O.; Lembke, D.; Kayci, M.; Radenovic, A.; Kis, A. Ultrasensitive Photodetectors Based on Monolayer MoS 2. *Nature Nanotechnology* **2013**, *8* (7), 497–501. https://doi.org/10.1038/nnano.2013.100.

(6) Huang, Y.; Guo, J.; Kang, Y.; Ai, Y.; Li, C. M. Two Dimensional Atomically Thin MoS2 Nanosheets and Their Sensing Applications. *Nanoscale*. Royal Society of Chemistry December 14, **2015**, pp 19358–19376. https://doi.org/10.1039/c5nr06144j.

(7) Li, H.; Yin, Z.; He, Q.; Li, H.; Huang, X.; Lu, G.; Fam, D. W.; Tok, A. I.; Zhang, Q.; Zhang, H. Fabrication of Single- and Multilayer MoS2 Film-Based Field-Effect Transistors for Sensing NO at Room Temperature. *Small* **2012**, *8* (1), 63–67. https://doi.org/10.1002/smll.201101016.

(8) Roy, K.; Padmanabhan, M.; Goswami, S.; Sai, T. P.; Ramalingam, G.; Raghavan, S.; Ghosh, A. Graphene-MoS 2 Hybrid Structures for Multifunctional Photoresponsive Memory Devices. *Nature Nanotechnology* **2013**, *8* (11), 826–830. https://doi.org/10.1038/nnano.2013.206.

(9) Schram, T.; Smets, Q.; Groven, B.; Heyne, M. H.; Kunnen, E.; Thiam, A.; Devriendt, K.; Delabie, A.; Lin, D.; Lux, M.; Chiappe, D.; Asselberghs, I.; Brus, S.; Huyghebaert, C.; Sayan, S.; Juncker, A.; Caymax, M.; Radu, I. P. WS2 Transistors on 300 Mm Wafers with BEOL Compatibility. *European Solid-State Device Research Conference* **2017**, 212–215. https://doi.org/10.1109/ESSDERC.2017.8066629.

(10) Lee, G. H.; Yu, Y. J.; Cui, X.; Petrone, N.; Lee, C. H.; Choi, M. S.; Lee, D. Y.; Lee, C.; Yoo, W. J.; Watanabe, K.; Taniguchi, T.; Nuckolls, C.; Kim, P.; Hone, J. Flexible and

Transparent MoS2 Field-Effect Transistors on Hexagonal Boron Nitride-Graphene Heterostructures. *ACS Nano* **2013**, *7* (9), 7931–7936. https://doi.org/10.1021/nn402954e.

(11) Coleman, J. N.; Lotya, M.; O'neill, A.; Bergin, S. D.; King, P. J.; Khan, U.; Young, K.; Gaucher, A.; De, S.; Smith, R. J.; Shvets, I. v; Arora, S. K.; Stanton, G.; Kim, H.-Y.; Lee, K.; Kim, G. T.; Duesberg, G. S.; Hallam, T.; Boland, J. J.; Wang, J. J.; Donegan, J. F.; Grunlan, J. C.; Moriarty, G.; Shmeliov, A.; Nicholls, R. J.; Perkins, J. M.; Grieveson, E. M.; Theuwissen, K.; Mccomb, D. W.; Nellist, P. D.; Nicolosi, V. *Two-Dimensional Nanosheets Produced by Liquid Exfoliation of Layered Materials*. *Science* **2011**, 331, 568-571. DOI: 10.1126/science.1194975

(12) Piao, M.; Chu, J.; Wang, X.; Chi, Y.; Zhang, H.; Li, C.; Shi, H.; Joo, M. K. Hydrothermal Synthesis of Stable Metallic 1T Phase WS2 Nanosheets for Thermoelectric Application. *Nanotechnology* **2018**, *29* (2). https://doi.org/10.1088/1361-6528/aa9bfe.

(13) Lauritsen, J. v; Kibsgaard, J.; Helveg, S.; Topsoe, H.; Clausen, B. S.; Laegsgaard, E.; Besenbacher, F. Size-Dependent Structure of MoS2 Nanocrystals. *Nature Nanotechnology* **2007**, *2* (1), 53–58. https://doi.org/10.1038/nnano.2006.171.

(14) Lin, Y. C.; Zhang, W.; Huang, J. K.; Liu, K. K.; Lee, Y. H.; Liang, C. T.; Chu, C. W.; Li, L. J. Wafer-Scale MoS2 Thin Layers Prepared by MoO3 Sulfurization. *Nanoscale* **2012**, *4* (20), 6637–6641. https://doi.org/10.1039/c2nr31833d.

(15) Li, Q.; Newberg, J. T.; Walter, E. C.; Hemminger, J. C.; Penner, R. M. Polycrystalline Molybdenum Disulfide (2H-MoS2) Nano- and Microribbons by Electrochemical/Chemical Synthesis. *Nano Letters* **2004**, *4* (2), 277–281. https://doi.org/10.1021/nl035011f.

(16) Yang, H.; Giri, A.; Moon, S.; Shin, S.; Myoung, J. M.; Jeong, U. Highly Scalable Synthesis of MoS2 Thin Films with Precise Thickness Control via Polymer-Assisted Deposition. *Chemistry of Materials* **2017**, *29* (14), 5772–5776. https://doi.org/10.1021/acs.chemmater.7b01605.

(17) Abbas, omar A.; Zeimpekis, I.; Wang, H.; Lewis, A. H.; Sessions, N. P.; ebert, M.; Aspiotis, N.; Huang, C.-C.; Hewak, D.; Mailis, S.; Sazio, pier. Solution-Based Synthesis of Few-Layer WS 2 Large Area Continuous Films for Electronic Applications. *Scientific Reports* **2020**, 10, 1696. https://doi.org/10.1038/s41598-020-58694-0.

(18) Lee, Y. H.; Zhang, X. Q.; Zhang, W.; Chang, M. T.; Lin, C. te; Chang, K. di; Yu, Y. C.; Wang, J. T. W.; Chang, C. S.; Li, L. J.; Lin, T. W. Synthesis of Large-Area MoS 2 Atomic Layers with Chemical Vapor Deposition. *Advanced Materials* **2012**, *24* (17), 2320–2325. https://doi.org/10.1002/adma.201104798.

(19) Tongay, S.; Fan, W.; Kang, J.; Park, J.; Koldemir, U.; Suh, J.; Narang, D. S.; Liu, K.; Ji, J.; Li, J.; Sinclair, R.; Wu, J. Tuning Interlayer Coupling in Large-Area Heterostructures with CVD-Grown MoS2 and WS2 Monolayers. *Nano Letters* **2014**, *14* (6), 3185–3190. https://doi.org/10.1021/nl500515q.

(20) Zhou, J.; Lin, J.; Huang, X.; Zhou, Y.; Chen, Y.; Xia, J.; Wang, H.; Xie, Y.; Yu, H.; Lei, J.; Wu, D.; Liu, F.; Fu, Q.; Zeng, Q.; Hsu, C. H.; Yang, C.; Lu, L.; Yu, T.; Shen, Z.; Lin, H.;

Yakobson, B. I.; Liu, Q.; Suenaga, K.; Liu, G.; Liu, Z. A Library of Atomically Thin Metal Chalcogenides. *Nature* **2018**, *556* (7701), 355–359. https://doi.org/10.1038/s41586-018-0008-3.

(21) Khan, K.; Tareen, A. K.; Aslam, M.; Wang, R.; Zhang, Y.; Mahmood, A.; Ouyang, Z.; Zhang, H.; Guo, Z. Recent Developments in Emerging Two-Dimensional Materials and Their Applications. *Journal of Materials Chemistry C* **2020**, *8* (2), 387–440. https://doi.org/10.1039/c9tc04187g.

(22) Huang, C. C.; Hewak, D. W.; Badding, J. v. Deposition and Characterization of Germanium Sulphide Glass Planar Waveguides. *Optics Express, Vol. 12, Issue 11, pp. 2501-2506* **2004**, *12* (11), 2501–2506. https://doi.org/10.1364/OPEX.12.002501.

(23) Huang, C. C.; Knight, K.; Hewak, D. W. Antimony Germanium Sulphide Amorphous Thin Films Fabricated by Chemical Vapour Deposition. *Optical Materials* **2007**, *29* (11), 1344–1347. https://doi.org/10.1016/j.optmat.2006.06.017.

(24) Huang, C. C.; Wu, C. C.; Knight, K.; Hewak, D. W. Optical Properties of CVD Grown Amorphous Ge-Sb-S Thin Films. *Journal of Non-Crystalline Solids* **2010**, *356* (4–5), 281–285. https://doi.org/10.1016/j.jnoncrysol.2009.12.027.

(25) Huang, C. C.; Al-Saab, F.; Wang, Y.; Ou, J. Y.; Walker, J. C.; Wang, S.; Gholipour, B.; Simpson, R. E.; Hewak, D. W. Scalable High-Mobility MoS2 Thin Films Fabricated by an Atmospheric Pressure Chemical Vapor Deposition Process at Ambient Temperature. *Nanoscale* **2014**, *6* (21), 12792–12797. https://doi.org/10.1039/c4nr04228j.

(26) Orsi Gordo, V.; Balanta, M. A. G.; Galvão Gobato, Y.; Covre, F. S.; Galeti, H. V. A.; Iikawa, F.; Couto, O. D. D.; Qu, F.; Henini, M.; Hewak, D. W.; Huang, C. C. Revealing the Nature of Lowerature Photoluminescence Peaks by Laser Treatment in van Der Waals Epitaxially Grown WS2 Monolayers. *Nanoscale* **2018**, *10* (10), 4807–4815. https://doi.org/10.1039/c8nr00719e.

(27) Felix, J. F.; da Silva, A. F.; da Silva, S. W.; Qu, F.; Qiu, B.; Ren, J.; de Azevedo, W. M.; Henini, M.; Huang, C. C. A Comprehensive Study on the Effects of Gamma Radiation on the Physical Properties of a Two-Dimensional WS2 Monolayer Semiconductor. *Nanoscale Horizons* **2020**, *5* (2), 259–267. https://doi.org/10.1039/c9nh00414a.

(28) Koma, A. *Van Der Waals Epitaxy for Highly Lattice-Mismatched Systems*. *Journal of Crystal Growth* **1999**; Vol. *201*, 236-241. https://doi.org/10.1016/S0022-0248(98)01329-3.

(29) Zhang, X.; Meng, F.; Christianson, J. R.; Arroyo-Torres, C.; Lukowski, M. A.; Liang, D.; Schmidt, J. R.; Jin, S. Vertical Heterostructures of Layered Metal Chalcogenides by van Der Waals Epitaxy. *Nano Letters* **2014**, *14* (6), 3047–3054. https://doi.org/10.1021/nl501000k.

(30) Miwa, J. A.; Dendzik, M.; Grønborg, S. S.; Bianchi, M.; Lauritsen, J. v.; Hofmann, P.; Ulstrup, S. Van Der Waals Epitaxy of Two-Dimensional MoS2-Graphene Heterostructures in Ultrahigh Vacuum. *ACS Nano* **2015**, *9* (6), 6502–6510. https://doi.org/10.1021/acsnano.5b02345.

(31) Lee, C.; Yan, H.; Brus, L. E.; Heinz, T. F.; Hone, J.; Ryu, S. Anomalous Lattice Vibrations of Single- and Few-Layer MoS2. *ACS Nano* **2010**, *4* (5), 2695–2700. https://doi.org/10.1021/nn1003937.

(32) Zhao, W.; Ghorannevis, Z.; Amara, K. K.; Pang, J. R.; Toh, M.; Zhang, X.; Kloc, C.; Tan, P. H.; Eda, G. Lattice Dynamics in Mono- and Few-Layer Sheets of WS2 and WSe2. *Nanoscale* **2013**, *5* (20), 9677–9683. https://doi.org/10.1039/c3nr03052k.

(33) McCreary, K. M.; Hanbicki, A. T.; Sivaram, S. v.; Jonker, B. T. A- and B-Exciton Photoluminescence Intensity Ratio as a Measure of Sample Quality for Transition Metal Dichalcogenide Monolayers. *APL Materials* **2018**, *6* (11). https://doi.org/10.1063/1.5053699.

(34) Chernikov, A.; Berkelbach, T. C.; Hill, H. M.; Rigosi, A.; Li, Y.; Aslan, O. B.; Reichman, D. R.; Hybertsen, M. S.; Heinz, T. F. Exciton Binding Energy and Nonhydrogenic Rydberg Series in Monolayer WS2. *Physical Review Letters* **2014**, *113* (7). https://doi.org/10.1103/PhysRevLett.113.076802.

(35) Lu, J.; Lu, J. H.; Liu, H.; Liu, B.; Chan, K. X.; Lin, J.; Chen, W.; Loh, K. P.; Sow, C. H. Improved Photoelectrical Properties of MoS2 Films after Laser Micromachining. *ACS Nano* **2014**, *8* (6), 6334–6343. https://doi.org/10.1021/nn501821z.

(36) Liu, W.; Benson, J.; Dawson, C.; Strudwick, A.; Raju, A. P. A.; Han, Y.; Li, M.; Papakonstantinou, P. The Effects of Exfoliation, Organic Solvents and Anodic Activation on the Catalytic Hydrogen Evolution Reaction of Tungsten Disulfide. *Nanoscale* **2017**, *9* (36), 13515–13526. https://doi.org/10.1039/c7nr04790h.

(37) Buscema, M.; Steele, G. A.; van der Zant, H. S. J.; Castellanos-Gomez, A. The Effect of the Substrate on the Raman and Photoluminescence Emission of Single-Layer MoS2. *Nano Research* **2014**, *7* (4), 561–571. https://doi.org/10.1007/s12274-014-0424-0.

(38) Wang, H.; Huang, C. C.; Polcar, T. Controllable Tunneling Triboelectrification of Two-Dimensional Chemical Vapor Deposited MoS2. *Scientific Reports* **2019**, *9* (1). https://doi.org/10.1038/s41598-018-36830-1.

(39) Cao, Y.; Wood, S.; Richheimer, F.; Blakesley, J.; Young, R. J.; Castro, F. A. Enhancing and Quantifying Spatial Homogeneity in Monolayer WS2. *Scientific Reports* **2021**, 11, 14831. https://doi.org/10.1038/s41598-021-94263-9.

Table of Contents (TOC) graphic: